Металлофиз. новейшие технол. / Metallofiz. Noveishie Tekhnol.
2016, т. 38, № 1, сс. 67–98 / DOI: 10.15407/MFiNT.38.0067

ДЕФЕКТЫ КРИСТАЛЛИЧЕСКОЙ РЕШЁТКИ

PACS numbers: 61.66.Dk, 61.72.J-, 61.72.Lk, 61.72.Nn, 62.20.mj, 62.20.mm, 64.75.Nx, 71.55.Ak

Carbon, Nitrogen, and Hydrogen in Iron-Based Solid Solutions: Similarities and Differences in Their Effect on Structure and Properties

V. G. Gavriljuk

G. V. Kurdyumov Institute for Metal Physics, N.A.S. of Ukraine,
36 Academician Vernadsky Blvd.,
UA-03680 Kyiv, Ukraine

Interstitial N, C and H atoms in iron-based solid solutions are compared in terms of their effect on the structure and properties. Electronic structure and stacking fault energy, atomic distribution, interaction of interstitial atoms with dislocations and vacancies, mobility of dislocations, mechanisms of deformation and fracture are compared based on theoretical calculations and experimental observations. As shown, nitrogen and hydrogen increase the electron density of states at the Fermi level of f.c.c. iron, whereas carbon decreases it. Correspondingly, the concentration of free electrons increases within the nitrogen and hydrogen iron-based solid solutions and decreases in the carbon ones. A correlation is revealed between the character of interatomic bonds and the short-range atomic order in the studied solid solutions: nitrogen assists short-range atomic ordering in the spatial distribution of alloying elements, whereas carbon promotes their clustering. As consequence, nitrogen increases thermodynamical stability of austenitic steels, whereas carbon makes steel sensitive to precipitation of carbides from the solid solution that deteriorates corrosive characteristics. The most impressive is a correlation between the change in the electronic structure and properties of dislocations. In contrast to prevailing covalent bonds in carbon steels, the enhanced metallic character of interatomic bonds, as caused by nitrogen, increases mobility of dislocations that results in excellent plasticity and fracture toughness. However, the same effect caused by hydrogen is a cause of the hydrogen embrittlement through the hydrogen-enhanced localized plas-

Corresponding author: Valentin Gennadievich Gavriljuk
E-mail: gavriljuk@rambler.ru

Please cite this article as: V. G. Gavriljuk, Carbon, Nitrogen, and Hydrogen in Iron-Based Solid Solutions: Similarities and Differences in Their Effect on Structure and Properties, *Metallofiz. Noveishie Tekhnol.*, **38**, No. 1: 67–98 (2016), DOI: 10.15407/MFiNT.38.0067.

ticity. A unique similarity with hydrogen embrittlement becomes apparent in the course of impact loading of austenitic nitrogen steels, where, due to the absence of sufficient time for relaxation of stresses, the nitrogen-enhanced localized plasticity occurs resulting in a pseudo-brittle fracture. The different is only the mechanism for localization of plastic deformation: the short-range atomic ordering caused by nitrogen and the increased concentration of superabundant vacancies due to hydrogen dissolution.

Key words: carbon, nitrogen, hydrogen, electronic structure, short-range atomic order, thermodynamical stability, deformation, fracture.

Проаналізовано вплив елементів втілення N, C і H в твердих розчинах на основі заліза на їхню структуру і властивості. На основі теоретичних розрахунків і експериментальних результатів порівнюються електронна структура і енергія дефектів пакування, розподіл атомів у твердих розчинах, взаємодія атомів втілення з дислокаціями та вакансіями, рухомість дислокацій, механізми пластичної деформації та руйнування. Встановлено, що Нітроґен і Гідроґен збільшують густину електронних станів на рівні Фермі ГЦК-заліза, в той час як Карбон зменшує її. Відповідно, концентрація вільних електронів підвищується в твердих розчинах Нітроґену і Гідроґену на основі γ-заліза і зменшується при розчиненні Карбону. Виявлено кореляцію між характером міжатомового зв'язку і близьким атомовим порядком в аустенітних сталях: Нітроґен сприяє близькому атомовому упорядкуванню в розподілі леґувальних елементів, в той час як розчинення Карбону супроводжується їх кластеризацією. Як наслідок, Нітроґен підвищує термодинамічну стабільність аустенітних сталей, а Карбон робить сталь чутливою до виділення карбідів із твердого розчину, що погіршує корозійні властивості. Найбільш вражаючою є кореляція між електронною структурою і властивостями дислокацій. На відміну від переважаючих ковалентних зв'язків у вуглецевих сталях, посилений Нітроґеном їхній металічний характер підвищує рухливість дислокацій, наслідком чого є висока пластичність і в'язкість руйнування. Але аналогічний вплив Гідроґену є причиною водневого окрихчування через посилену Гідроґеном локалізовану пластичність. Унікальна схожість з водневим окрихчуванням має місце, якщо аустенітна азотиста сталь піддається ударному навантаженню. Внаслідок недостатнього часу для релаксації напружень, посилена Нітроґеном локалізована пластичність призводить до псевдокрихкого руйнування. Відмінним є лише механізм локалізації пластичної деформації: близьке атомове упорядкування, спричинене Гідроґеном, і збільшення концентрації надлишкових вакансій у випадку розчинення Гідроґену.

Ключові слова: сталь, Карбон, Нітроґен, Гідроґен, електронна структура, близький атомовий порядок, термодинамічна стабільність, деформація, руйнування.

Выполнен анализ влияния элементов внедрения N, C и H в твёрдых растворах на основе железа на их структуру и свойства. На основе теоретических расчётов и экспериментальных данных сравниваются электронная структура и энергия дефектов упаковки, распределение атомов в твёрдых

растворах, взаимодействие атомов внедрения с дислокациями и вакансиями, подвижность дислокаций, механизмы пластической деформации и разрушения. Установлено, что азот и водород повышают плотность электронных состояний на уровне Ферми ГЦК-железа, в то время как углерод уменьшает её. Соответственно, концентрация свободных электронов увеличивается в твёрдых растворах азота и водорода на основе γ-железа и уменьшается при растворении углерода. Найдена корреляция между характером межатомных связей и ближним атомным порядком в аустенитных сталях: азот способствует ближнему атомному упорядочению в распределении легирующих элементов, в то время как растворение углерода сопровождается их кластеризацией. Как следствие, азот увеличивает термодинамическую стабильность аустенитных сталей, а углерод делает сталь чувствительной к выделению карбидов из твёрдого раствора, что ухудшает коррозионные свойства. Наиболее впечатляющей является корреляция между электронной структурой и свойствами дислокаций. В отличие от превалирующих ковалентных связей в углеродистых сталях, усиленный азотом их металлический характер увеличивает подвижность дислокаций, следствием чего является высокая пластичность и вязкость разрушения. Однако аналогичное влияние водорода является причиной водородного охрупчивания стали из-за усиленной водородом локализованной пластичности. Уникальное сходство с водородной хрупкостью имеет место, если аустенитная азотистая сталь подвергается ударному нагружению. Вследствие недостаточного времени для релаксации напряжений, усиленная азотом локализованная пластичность приводит к псевдохрупкому разрушению. Различным является лишь механизм локализации пластической деформации: ближнее атомное упорядочение, обусловленное азотом, и повышение концентрации избыточных вакансий в случае растворения водорода.

Ключевые слова: сталь, углерод, азот, водород, электронная структура, ближний атомный порядок, термодинамическая стабильность, деформация, разрушение.

(Received December 18, 2016)

1. INTRODUCTION

The carbon, nitrogen, and hydrogen solid solutions in the iron-based alloys are characterized by different limits of solubility depending on the crystal modification of the iron (α, γ, ε) and content of substitutional alloying elements. As compared to carbon, nitrogen positively affects mechanical and chemical properties of austenitic steels and, be bound in carbonitrides, is effective for design of high strength low-alloyed steels (HSLA). Carbon causes a number of harmful effects in austenitic steels, particularly those concerned with brittle fracture and bad corrosion resistance (see, *e.g.*, [1, 2]). Studies of hydrogen in steel are usually concerned with hydrogen brittleness, of which mechanism is still the subject of discussion (see reviews in [3–6]).

So far, hydrogen effects in the iron-based solid solutions were not compared with those of carbon or nitrogen. The aim of this article is to fill this gap and discuss similarities and differences between C, N and H in steel starting up from the atomic interactions, and consider possible consequences for thermodynamic stability of solid solutions, interaction with the crystal lattice defects and mechanical properties.

It is generally accepted that 'structure' stands for crystal lattice, lattice defects and their distribution as well as for grain size. In the solid solutions, the type of solute atoms and their distribution, as well as precipitates are taken into account.

In fact, the structure of metals and alloys starts from localized or free electrons. Under external force and resultant straining, the atoms are being shifted from their positions, and mechanical response, plastic deformation or brittle fracture, depends on the character of interatomic bonds. In comparison with the nuclei, the response of electrons is quicker by many orders of magnitude. The closed electron shell, so-called 'ion core', can be excluded from the consideration because it does not take part in chemical reactions and, under straining, can be only slightly deformed, *i.e.*, polarized. Only the external, *i.e.*, valence electrons are responsible for chemical bonds and deformation behaviour.

The prevailing localized valence electrons form covalent bonds between the atoms in the crystal lattice, which causes brittleness because even a slight shift of the atoms under shear stress in the slip plane leads to breaking the interatomic bonds. This is, *e.g.*, the case of the transition metals and alloys of group V and VI in the periodic table (Cr, Mo, V, Nb, W). Free electrons are responsible for the metallic character of interatomic bonds, and the higher their fraction is the more ductile are metals and alloys.

In relation to phase transformations, valence electrons are responsible for the height of the energy barrier, which have to be overcome by the atoms constituting a new crystal lattice, either during its nucleation or during their jumps through the interface between matrix and new phase. Again, the stronger the covalent bonds between the atoms are, the higher this energy barrier is. For this reason, the transition metals of group V and VI do not reveal any polymorphic transformations.

Moreover, as will be shown, the control of interatomic bonds and the free/localized electron ratio affects short-range atomic order in multicomponent solid solutions and, for this reason, their thermodynamic stability.

2. ATOMIC INTERACTIONS

Ab initio calculations of the electronic structure in the f.c.c. iron containing carbon, nitrogen or hydrogen, as studied in [7–9], have shown

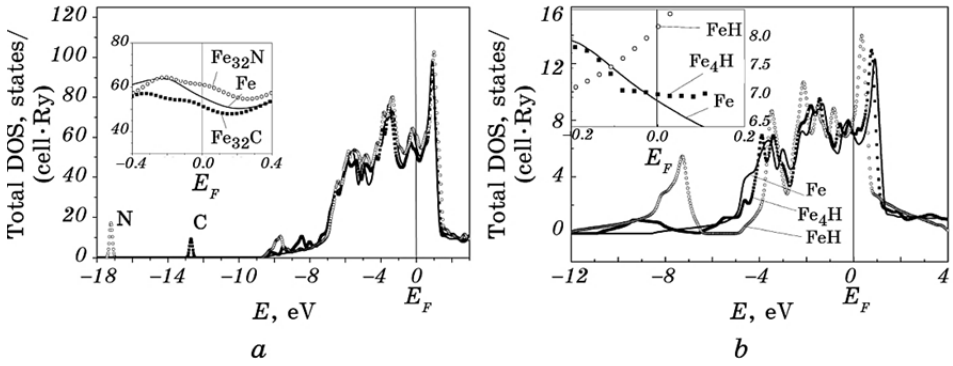

Fig. 1. Density of electron states per elementary cell in the f.c.c. iron and iron-based solid solutions: $Fe_{32}C$ and $Fe_{32}N$ (*a*), Fe_4H and FeH (*b*). The situation at the Fermi level is shown in the insert at the left upper corners.

that carbon decreases density of electron states at the Fermi level of f.c.c. iron, whereas nitrogen and hydrogen increase it (Fig. 1). In other words, carbon is expected to promote the covalent character of interatomic bonds, whereas nitrogen and hydrogen assist prevailing metallic bonds between atoms.

This result is consistent with the experimental data obtained using conduction electron spin resonance [10–13]). According to data in Fig. 2, *a*, the alloying of austenitic steels with nitrogen increases the concentration of free electrons at the Fermi level. In its influence on the electronic structure of the γ-iron, hydrogen is similar to nitrogen. Shown in Fig. 2, *b* is the spectrum of electron spin resonance in $Cr_{18}Mn_{20}N_{0.88}$ (% mass) hydrogen-charged and hydrogen-free austenitic steel. The Ni-free steel was chosen in this experiment because, in presence of nickel, the hydrogen charging causes ferromagnetism, which makes impossible the observation of the ESR signal. Nitrogen in this steel was introduced to provide stability of the austenitic phase at temperatures down to 4.2 K. The obtained data confirm that, like nitrogen, hydrogen increases the concentration of free electrons at the Fermi level.

Free electrons in nitrogen austenitic steels markedly contribute to the magnetic susceptibility (Pauli paramagnetism), by more than one order of the value larger in the comparison with carbon steels. In contrast, the localization of electrons at the atomic sites contributing to the Curie–Weiss magnetic susceptibility is more pronounced in the carbon steels (see Table 1).

In many relations, it is particularly important to know the spatial distribution of the electron density over the crystal lattice. As an example, Fig. 3 shows some results of *ab initio* calculations concerning the distribution of external electrons (*i.e.* except for the electrons of

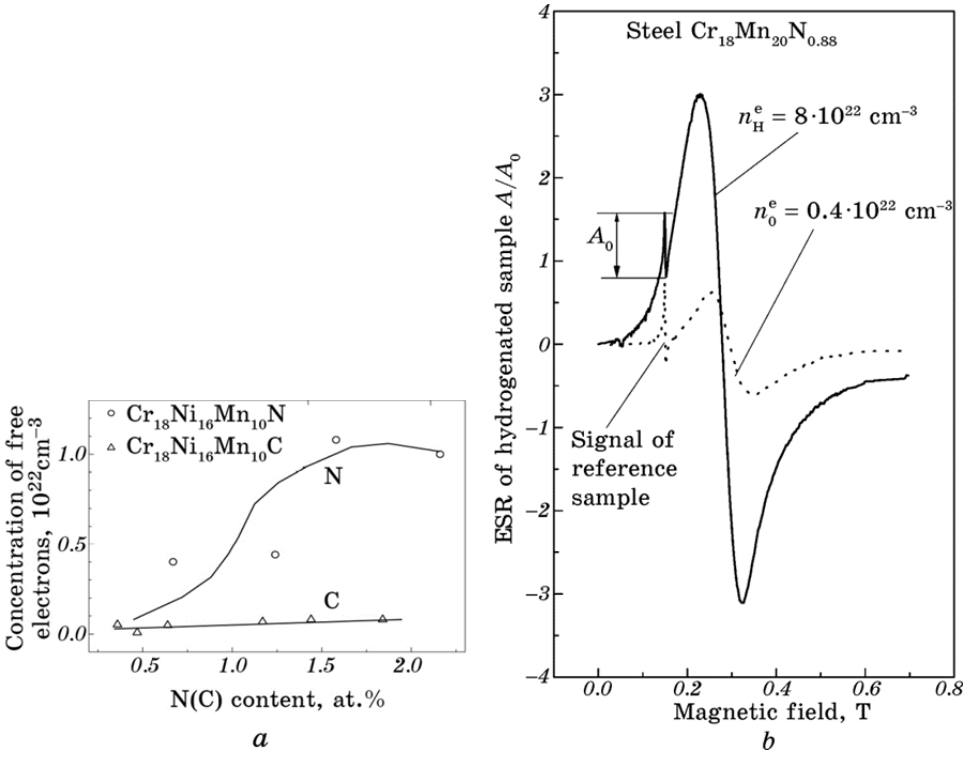

Fig. 2. Concentration of free electrons at the Fermi level in the austenitic steels alloyed with carbon and nitrogen (*a*) and signal of electron spin resonance in the hydrogen-free and hydrogen-charged steel $Cr_{18}Mn_{10}N_{0.88}$ (*b*). A piece of the borate glass having 10^{15} spins was used as a reference sample for determination of spin concentration. The intensity of ESR signal is normalized to that of the reference sample A_0.

the ion cores) in the octahedral sites of the γ-iron f.c.c. lattice occupied by carbon, nitrogen or hydrogen atoms. It is seen that the electrons are substantially removed from the interstitial site in the case of carbon, whereas their density increases in the vicinity of nitrogen or hydrogen atom located in the interstitial sites. These results suggest that carbon ions in the austenite are positively charged, whereas nitrogen and hydrogen ions carry an effective negative electric charge.

Let us compare the results of these calculations with available experimental data. The measurements of the electron transfer in the binary Fe–C and Fe–N austenites [14, 15] have given the evidence that carbon atoms in the γ-iron solid solution carry a positive electric charge, whereas nitrogen atoms are likely to be negatively charged. The data in Fig. 3 allow explaining such a different behaviour. The increased concentration of free electrons at the interstitial sites occupied

TABLE 1. Some parameters of atomic interactions in $Cr_{18}Ni_{16}Mn_{10}$ steels containing nitrogen or carbon: χ_{c0}, χ_{d1} are magnetic susceptibilities of free electron (Pauli paramagnetism) and isolated *d*-electron (Curie–Weiss) subsystems; Θ is the energy of superparamagnetic (Langevin) clusters in the temperature units characterising the size of clusters.

Steel	N(C) content, % mass	$10^7 \cdot \chi_{c0}$	$10^5 \cdot \chi_{d1}$	Θ, K
N1	0.17	4.0	2.2	140
N2	0.4	10.8	0.9	140
C1	0.15	0.4	13.7	315
C2	0.43	0.8	80.0	715

by the nitrogen atoms in the f.c.c. iron is consistent with the negative effective charge. The positive effective charge of the carbon atoms follows from the decrease in the electron concentration at the site occupied by carbon atoms as compared to that in the interstitial-free site. Measurements of ESR evidence an increase in the concentration of the localised *d*-electrons due to carbon in comparison with nitrogen in the f.c.c. iron (see Table 1). Experimental data about the charge of hydrogen atoms in metals are controversial. The *ab initio* calculations support the idea of their negative effective charge.

3. ATOMIC DISTRIBUTION

A correlation between the character of interatomic bonds (the states density and, correspondingly, the concentration of free electrons at the Fermi level) and the atomic distribution in the iron-based solid solutions has been found based on the experimental data obtained using Mössbauer spectroscopy, electron spin resonance and small angle scattering of neutrons.

3.1. Mössbauer spectroscopy is a useful tool for studying the short-range atomic order in iron-based solid solutions due to its high resolution in the identification of different atomic configurations in the crystal lattice [16–18].

Mössbauer spectra of binary Fe–C and Fe–N solid solutions and corresponding atomic configurations are presented in Fig. 4. The Fe–C spectrum consists of a single line belonging to iron atoms Fe_0 having no carbon atoms as nearest neighbours. The doublet comes from the iron atoms Fe_1 with one carbon atom as nearest neighbour and Fe_{2-90° with two carbon atoms in the nearest interstitial sites. These two different configurations cause the same electric field gradient in the crystal lattice (only its sign is different), which results in the same quadrupole splitting of the spectrum.

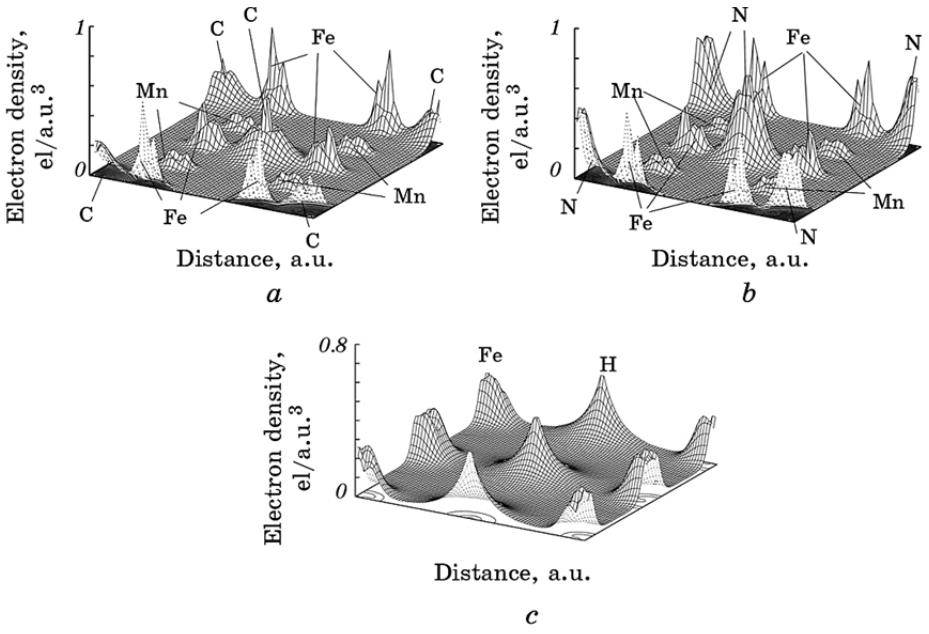

Fig. 3. Spatial distribution of the valence electron density along (110) plane in the lattice of solid solutions: $Fe_{20}Mn_8Cr_4C_2$ (*a*), $Fe_{20}Mn_8Cr_4N_2$ (*b*), FeH (*c*).

Such 90°-pairs are never met in the Fe–N austenite. Instead, in addition to the Fe_1 component caused by single nitrogen atoms, the spectrum contains a doublet from the $Fe_{2-180°}$ configurations caused by nitrogen atoms occupying interstitial sites within the second coordination sphere in the interstitial sublattice. Such a dumbbell-like configuration is an element of the ordered Fe_4N γ'-phase.

In order to obtain the values of C–C and N–N interaction energies, which could be consistent with the fractions of atomic configurations derived from Mössbauer spectra, a modelling of these solid solutions was carried out using the Monte Carlo method (Fig. 5). W_1 and W_2 are the energies of interaction between any two interstitial atoms in the first and second coordination spheres, respectively, under condition that one of them is located in the co-ordinate origin. The areas marked as C–C and N–N correspond to the values of C–C and N–N interactions which are consistent with the fractions Fe_1 (*d*), $Fe_{2-90°}$ (*e*) and $Fe_{2-180°}$ (*f*) atoms in Fig. 4.

It is seen from Fig. 5 that the carbon distribution in austenitic steels is characterized by a soft repulsion between C atoms in nearest interstitial sites (a small W_1 for the C–C area), so that, along with single carbon atoms, some fraction of carbon pairs $Fe_{2-90°}$ can exist. However, a hard C–C repulsion (large W_2) is revealed for carbon atoms as the neighbours in the second coordination sphere of the interstitial sublat-

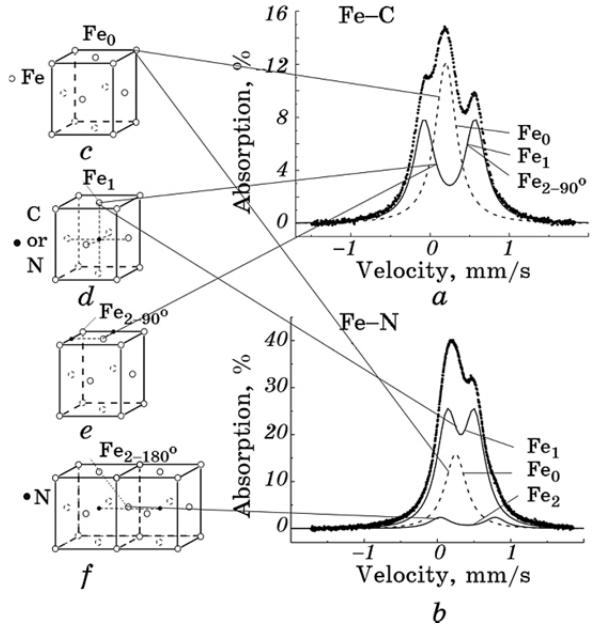

Fig. 4. Mössbauer spectra of binary austenitic solid solutions, at.%: Fe–9.1C (*a*), Fe–9.3N (*b*) and corresponding atomic configurations(*c*–*f*).

tice. This means that dumbbell-like C–Fe–C configurations Fe_{2-180° do not exist in the austenitic carbon steels, which makes impossible the existence of an ordered Fe_4C type structure.

In contrast, the N–N repulsion in the first coordination sphere is so hard (large W_1) that nitrogen atoms cannot be nearest neighbours in the austenitic lattice, whereas the soft repulsion in the second coordination sphere (small W_2) allows the N–Fe–N pairs which are clearly identified in the Mössbauer spectra of austenitic nitrogen steels. This is why the distribution of nitrogen atoms is characterized by short-range atomic ordering. The carbon atoms in austenitic steels are prone to form clusters.

The comparison of these experimental data with the aforementioned effect of carbon and nitrogen on the electronic structure of the iron austenite provides one with a suggestion that the increase in the states' density, *i.e.* the increased concentration of free electrons at the Fermi level, assists the short-range atomic ordering, whereas the localization of electrons at the atomic sites promotes clustering of solute atoms [19].

This idea was confirmed in subsequent studies of combined alloying of austenitic steels with carbon and nitrogen and development of a new class of high-strength corrosion-resistant austenitic steels [2, 20, 21]. Mössbauer studies of the ternary Fe–0.9C–0.9N alloy have shown that

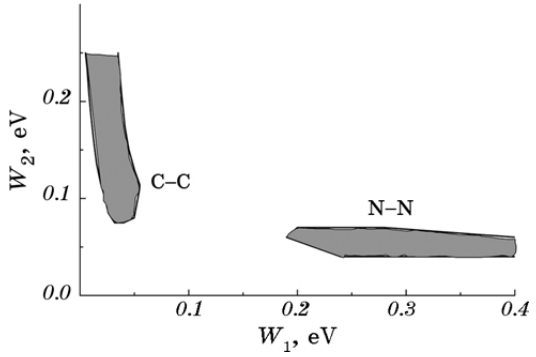

Fig. 5. Areas of C–C and N–N atomic interactions (marked with grey colour) within the first and second coordination spheres on the sublattice of interstitial sites corresponding to the fractions of Fe_1 (*d*), Fe_{2-90° (*e*) and Fe_{2-180° (*f*) iron atoms obtained from Mössbauer spectra in Fig. 4.

this change in the electronic structure results in an unordinary distribution of the interstitial atoms in the solid solution, namely in the tendency to not occupy the sites within the first two coordination spheres of the interstitial sublattice. The experimental evidence for that is presented in Fig. 6. The spectrum consists of the austenitic and martensitic parts. In contrast to the Fe–N austenite, the austenitic component does not contain the doublet with the double quadrupole splitting from dumbbell-like N–Fe–N nitrogen configurations (compare with Fig. 4, *b*, *f*), and there is no component from 90° Fe_2 carbon configurations in the martensitic part, which is typical for Fe–C martensite (see the Fe–C martensite spectrum in the upper right corner).

Mössbauer studies have also shown that carbon and nitrogen affect the distribution of substitutional solutes in the multicomponent iron-based alloys. The outer lines of the ferritic spectra of steels with basic $Cr_{15}Mo_1$ composition containing carbon, nitrogen or carbon + nitrogen are presented in Fig. 7. After quenching, these steels were subjected to tempering at 500°C, so that carbon is not present in the solid solution. The occurrence of carbides cannot affect the outer lines of the ferritic spectra because the hyperfine field on the iron nuclei in the carbides is much smaller in comparison with that in the ferrite.

Four components from the iron atoms having no, one, two and three substitutional atoms as nearest neighbours can be distinguished in the spectra presented in Fig. 7. The component Fe_0 is clearly resolved and can be properly used for the analysis. It is seen that the replacement of carbon by nitrogen decreases the fraction of Fe_0 atoms, which suggests a more homogeneous distribution of the substitutional atoms. The smallest fraction of the iron atoms not having neighbouring substitutional atoms is found in the C + N alloy and, therefore, the combined

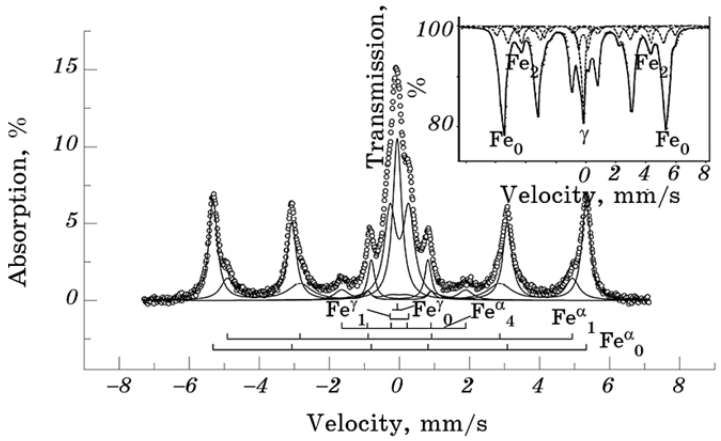

Fig. 6. Mössbauer spectrum of Fe–0.93C–0.91N (% mass) solid solution. For the comparison, the Fe–C spectrum is shown in the upper right corner.

C + N alloying retards clustering of chromium (molybdenum) atoms and provides the most homogeneous atomic distribution.

3.2. Electron spin resonance (ESR). Three electron subsystems contribute to the magnetic susceptibility in the iron-based solid solutions: (i) the conduction (free) electrons denoted as *c*-subsystem (Pauli paramagnetism), (ii) localized *d*-electrons named in the following as *d1*-subsystem (Curie–Weiss paramagnetism) and (iii) clusters of *d*-atoms acquiring their macroscopic moments due to spin polarisation (Langevin superparamagnetism) denoted as *d2*-subsystem. The temperature dependence of the ESR signal parameters was obtained from measurements in [10] using a theory [22], which takes into account the exchange interaction between the free electrons (*c*-subsystem) and the *d1*-, *d2*-subsystems.

As a result of this exchange (see for details [10]), magnetic susceptibilities of *c*- and *d*-electron subsystems are

$$\chi_c = \chi_{c0}(1 + \alpha\chi_d), \qquad (1)$$
$$\chi_d = \chi_{d0}(1 + \alpha\chi_{c0}),$$

where α is an exchange parameter, and χ_d is the magnetic susceptibility of *d1*-, *d2*-subsystems.

The magnetic susceptibility χ_{c0} of free electron subsystem not interacting with *d*-subsystems is described as

$$\chi_{c0} = (1/2)g^2\mu_B^2 D_F, \qquad (2)$$

where *g* is the spectroscopic factor characterising a splitting of the

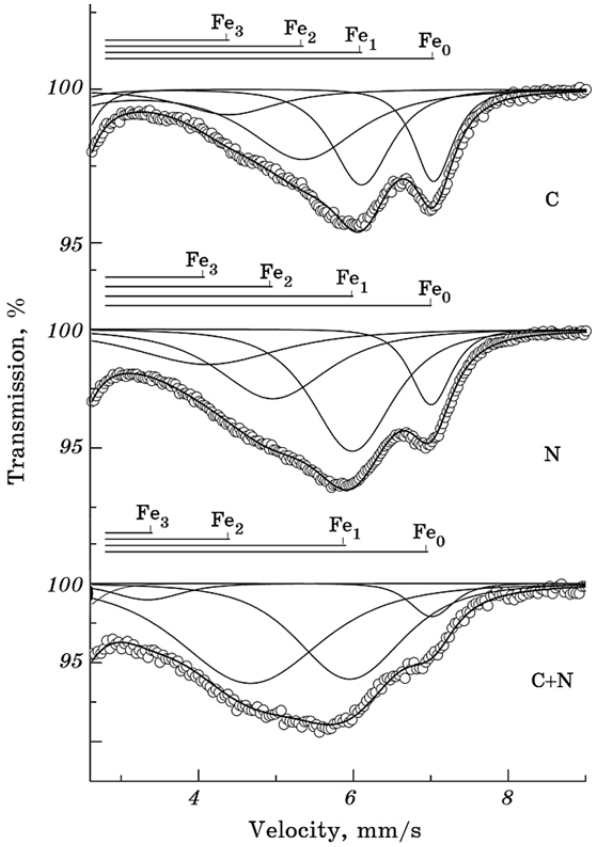

Fig. 7. Outer lines of Mössbauer spectra of steels with (% mass) 15 Cr, 1 Mo and 0.6 C or 0.62 N or 0.35 N + 0.29 C after quenching from 1100°C and tempering at 650°C for 2 hours.

electron levels under applied magnetic field, and it is determined from the CESR spectra, μ_B is the Bohr magneton, D_F is the state density at the Fermi level with energy $E = E_F$.

The value of χ_{c0} does not depend on the temperature in the low-temperature range $k_B T << E_F$. As was mentioned above, there are two contributions to the magnetic susceptibility χ_d:

$$\alpha\chi_d = \alpha_1\chi_{d1} + \alpha_2\chi_{d2}. \tag{3}$$

The magnetic susceptibility of the isolated localized d-electrons χ_{d1} changes with the temperature according to the Curie–Weiss law:

$$\chi_{d1}(T) = C_1/T, \tag{4}$$

and the magnetic susceptibility of superparamagnetic clusters obeys the Langevin law:

$$\chi_{d2}(T) = C_2 L(\Theta/T),\ C_2 = \chi_{d2} \text{ at } T = 1, \qquad (5)$$
$$L(\Theta/T) = \coth(\Theta/T) - T/\Theta,$$
$$\Theta = MH/k_B,$$

where M is the cluster magnetic moment, H is the external magnetic field, k_B is the Boltzmann constant, Θ is the energy of cluster in the magnetic field in the temperature units, and it is proportional to the number of d-atoms in the cluster.

The relation between $g(T)$ and magnetic susceptibilities is written as

$$g(T) = g_c(1 + \chi_r^{-1}(T))/(g_c / g_{d1} + \chi_r^{-1}(T)), \qquad (6)$$

where the relative magnetic susceptibility $\chi_r^{-1}(T)$ consists of three above-mentioned contributions in a paramagnetic alloy:

$$\chi_r^{-1}(T) = \chi_c / \chi_{d1} = \alpha_1\chi_{c0} + \chi_{c0}\chi_{d1}^{-1} + \alpha_2\chi_{d2}\chi_{c0}\chi_{d1}^{-1}. \qquad (6)$$

Figure 8, see also Table 1, shows the temperature dependence of χ_r^{-1} for austenitic steels $Cr_{18}Ni_{16}Mn_{10}C$ containing 0.15% or 0.43% of carbon and $Cr_{18}Ni_{16}Mn_{10}N_{0.4}$ (% mass). It is seen that the Curie–Weiss law profoundly determines the $\chi_r^{-1}(T)$ behaviour in the nitrogen-containing steels, which suggests a preference of single d-atoms in the solid solution. In contrast, the Langevin superparamagnetism controls $\chi_r^{-1}(T)$, if nitrogen is replaced by carbon, *i.e.* the clusters of d-atoms prevail in the carbon austenitic steel.

The size of clusters can be estimated on the value of Θ if some average value of the magnetic moment for each d-atom, *e.g.* $\cong 2.5\mu_B$, is suggested. Then, using the relation $\Theta = MH/k_B$, where $M = g\mu_B N_a$, and the value of the external magnetic field $H = 0.3$ T used in the experiment, one obtain the number of d-atoms in the cluster, $N_a \approx \Theta$, which corresponds to an average size of clusters in the carbon austenitic steels of about 1 to 2 nm.

3.3. Small-angle scattering of neutrons. Experimental observations of the nitrogen and carbon effects on the distribution of alloying elements in austenitic steels were performed using the small angle neutron scattering, SANS [23]. This method allows one to obtain the information concerning the mass (chemical) inhomogeneities in solid solutions on the scale of several tens nm. An incident neutron beam is scattered on the inhomogeneities of mass distribution in the sample and the weakening of its intensity is described as the total cross section of scattering $S_{tot} = \ln(I_0/I)$, where I_0 and I are the intensities of the in-

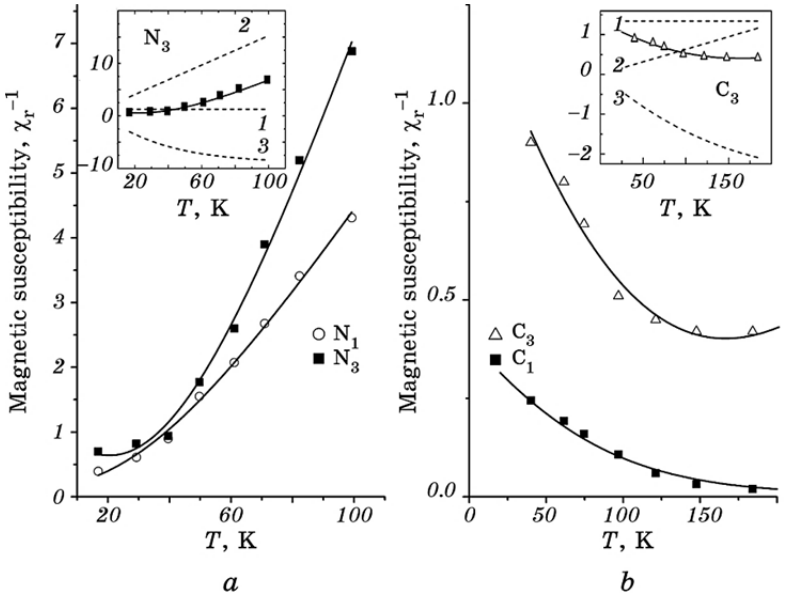

Fig. 8. Temperature dependence of magnetic susceptibility of austenitic steels $Cr_{18}Ni_{16}Mn_{10}N_{0.4}$ and $Cr_{18}Ni_{16}Mn_{10}C_{0.43}$ (% mass). The fitting of experimental data to formula (7) is shown by solid lines. The insert shows contributions to the magnetic susceptibility from free electrons (*1*), localized *d*-electrons (*2*) and superparamagnetic clusters (*3*) as obtained from the fitting. Deviation from the linear relation (Curie–Weiss law) is caused by the superparamagnetic clusters of substitutional solute atoms.

cident and passed neutron beams, respectively (see Fig. 9). As the nuclei of different elements differ in their neutron scatterings (the scattering lengths for chromium $b_{Cr} = 0.352 \cdot 10^{-12}$ cm, manganese $b_{Mn} = -0.36 \cdot 10^{-12}$ cm, iron $b_{Fe} = 0.96 \cdot 10^{-12}$ cm, nickel $b_{Ni} = 1.03 \cdot 10^{-12}$ cm, $b_C = 0.66 \cdot 10^{-12}$ cm, $b_N = 0.94 \cdot 10^{-12}$ cm, see in detail [24]), the atomic clusters have to enhance the neutron scattering.

As follows from Fig. 9, the alloying of austenitic CrNi and CrNiMn steels with nitrogen decreases the total cross section of neutron scattering, whereas carbon causes a striking increase of S_{tot}.

It has to be emphasised that this effect is not due to scatterings of neutrons on nitrogen or carbon atoms themselves because, if it would be the case, the opposite effect is expected as the scattering cross section of neutrons on the nitrogen atoms is about twice and the absorption cross section is more than 500 times as large as those on the carbon ones.

Moreover, the fractions of nitrogen and carbon atoms in solid solutions are too small in order to cause such a large scattering. Therefore, it is an effect of nitrogen and carbon on the distribution of substitu-

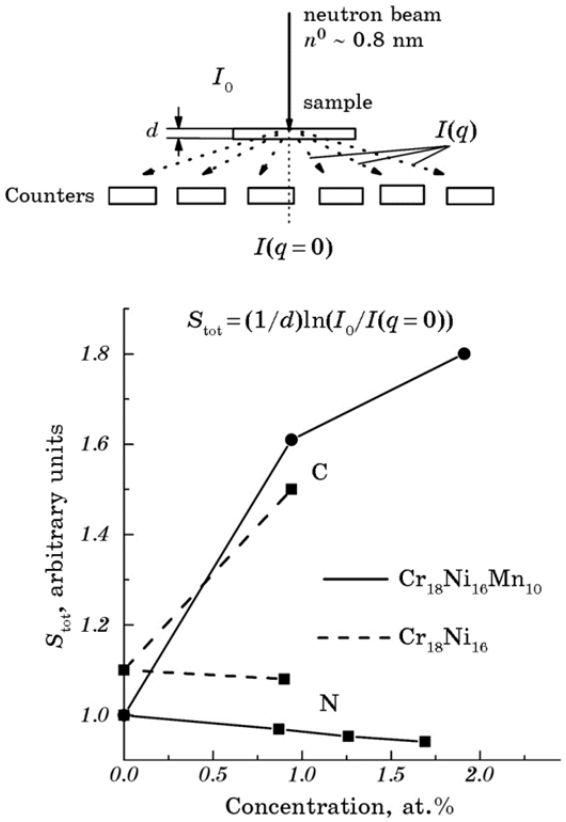

Fig. 9. A scheme of small angle neutron scattering measurements and an effect of nitrogen and carbon on the total cross section of neutron scattering S_{tot} in the austenitic $Cr_{18}Ni_{16}Mn_{10}$ and $Cr_{18}Ni_{16}$ steels. The wavelength of neutrons is about 0.8 nm; S_{tot} is measured as a weakening of the intensity I_0 of the primary neutron beam.

tional solutes, *i.e.* on the short-range atomic order in austenitic steels.

Based on the presented results, one can conclude that a clear tendency to clustering is observed in the carbon-containing steels, whereas the short-range atomic ordering occurs, if carbon is replaced by nitrogen in the steels of the same basic composition.

A reason for this striking difference between carbon and nitrogen effects is attributed to the nitrogen-enhanced metallic character of interatomic bonds and prevailing covalent bonds due to carbon [19]. Such a correlation between the electronic structure and atomic distribution was also observed in the variety of substitutional iron-based alloys [25], where it was established that the increase in the concentration of Cr, Mn, Mo, V leads to prevailing localization of electrons at the atomic sites and assists clustering in the solid solutions, whereas alloying by

Ni, Si, Al increases the concentration of free electrons at the Fermi level and promotes short-range atomic ordering.

Hydrogen in steels cannot affect the distribution of substitutional solutes because the hydrogenation usually proceeds at ambient temperature, and heating is accompanied by hydrogen degassing. Possibly, the effect of hydrogen on the atomic distribution can be found in the Ti alloys where solubility of hydrogen at high temperatures is remarkable.

4. THERMODYNAMIC STABILITY

As well known, carbon negatively affects properties of CrNi and CrMn austenitic steels because of easy precipitation and difficult dissolution of chromium carbides. Substitution of carbon by nitrogen increases thermodynamic stability of austenitic steels, which can be attributed to the nitrogen-caused short-range atomic ordering. First of all, the solubility of nitrogen in the iron austenite is increased as compared to carbon allowing the significant solid solution strengthening. Beside this, nitrogen in austenitic steels retards the precipitation of intermetallic phases during the sensitisation treatments (see, *e.g.*, [26–29]).

On the other hand, nitrogen is more effective in stabilizing the austenitic structure in relation to martensitic transformation [30]. As shown in Fig. 10, *a*, *b*, after quenching of the chromium steel Cr15Mo1, the fraction of the retained austenite increases if carbon is replaced by nitrogen. The combined alloying with carbon + nitrogen provides the highest stability of austenite (Fig. 8, *c*).

The atomic distribution in austenite is inherited by the as-quenched martensite and, as a result, the precipitation during tempering is also shifted to higher temperatures in the same order: carbon → nitrogen → → carbon + nitrogen, which was established in TEM studies [31]. Dilatometric curves presented in Fig. 11 illustrate the delay of the 1st and 3rd transformations during tempering, as well as the retardation of the retained austenite decomposition (2nd one) caused by nitrogen- and nitrogen + carbon. This is expected taking into account the high concentration of free electrons at the Fermi level and the corresponding short-range atomic order.

Hydrogen in austenitic steels is also found to affect thermodynamic stability. It is established that hydrogen charging of austenitic steels causes the $\gamma \rightarrow \varepsilon$ transformation (*e.g.* [32–34]). Very often, this transformation is attributed to the hydrogen-induced defects and stresses as it occurs during the cold work of austenitic steels. At the same time, the calculations of the electronic structure show [35, 36] that, with extremely high hydrogen contents, the cohesive energy in the h.c.p. iron lattice increases in relation to that in the f.c.c. one in the absence of any stresses, which suggests that hydrogen makes preferential the

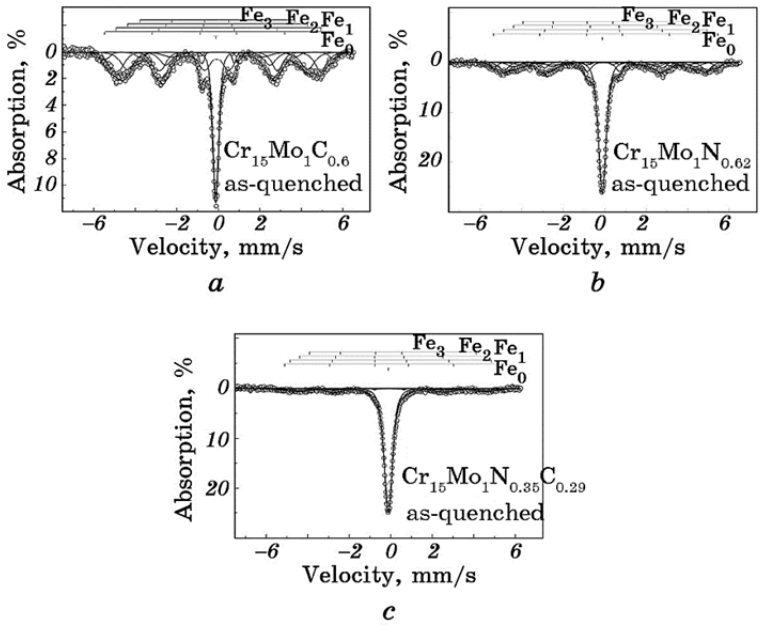

Fig. 10. Mössbauer spectra of as-quenched steel $Cr_{15}Mo_1$ alloyed with (% mass) 0.6C (*a*), 0.62N (*b*) or 0.29C + 0.35N (*c*). A single line belongs to the iron atoms in the paramagnetic retained austenite. The sextet consisting of four components Fe_0 to Fe_3 arises from the iron atoms in the ferromagnetic martensite having a different chromium neighbourhood.

h.c.p. lattice of the ε-phase.

The common feature in the nitrogen and hydrogen effects on the thermodynamical stability of austenite is that, at high N and H contents, the h.c.p. lattice becomes more stable than the f.c.c. one and the h.c.p. ε-phase exists within the wide concentration range of nitrogen or hydrogen.

5. CRYSTAL LATTICE IMPERFECTIONS

5.1. Stacking fault energy. As shown first time in [37], the stacking fault energy (SFE) in pure metals is inversely proportional to the states density at the Fermi level. Deviations from this rule are observed in the solid solutions if the constituting elements are located far from each other in the periodic table. This correlation can be observed for carbon and hydrogen in austenitic steels: the carbon-caused decrease in the concentration of free electrons corresponds to increasing SFE [38], whereas the hydrogen-increased concentration of free electrons correlates with decreasing SFE [39].

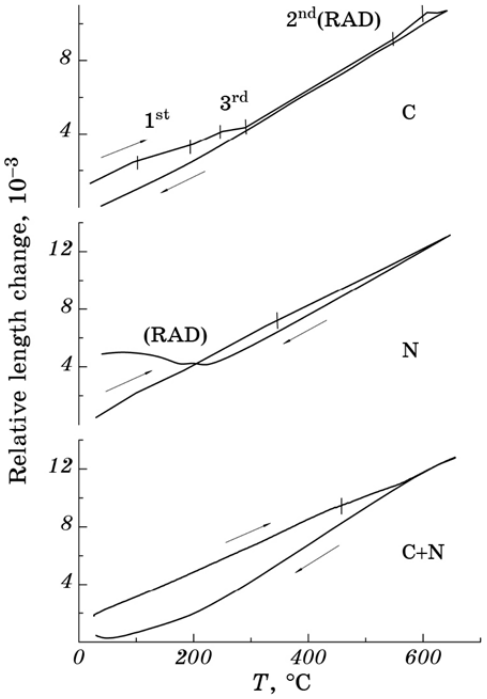

Fig. 11. Length change during tempering of martensitic steels $Cr_{15}Mo_1N_{0.62}$, $Cr_{15}Mo_1C_{0.6}$ and $Cr_{15}Mo_1N_{0.35}C_{0.29}$ quenched in water from 1100°C. The temperature ranges of the 1st (precipitation of low-temperature carbides or nitrides), 2nd (decomposition of retained austenite) and 3rd (precipitation of stable carbide/nitride phases) transformations during tempering are marked.

Some uncertainty exists in relation to nitrogen in austenite. Fawley *et al.* [40] observed a slightly decreasing effect on the SFE (from 40 to 38 mJ/m^2) caused by the variation of nitrogen content within 0.005–0.05% mass in steel $Cr_{20}Ni_{20}$. Swann [41] has shown that the addition of 0.12% mass of nitrogen to the steel $Cr_{18}Ni_{13}$ results in slight lowering SFE. Dulieu and Nutting [42] obtained nearly the same result in TEM studies of the steel $Cr_{18}Ni_{10}$. An increase in the nitrogen content from 0.02% to 0.25% mass produced decreasing the SFE. Stoltz and Vander Sande [43] found a decrease of the SFE due to nitrogen in austenitic CrNiMn steels. A feature of their observations was that an increase of the nitrogen content above 0.24% mass did not affect the SFE.

A non-monotonous SFE concentration behaviour was found in studies [44], and a direct proportionality between the SFE and concentration of free electrons was observed. However, the measurements of the temperature dependence of SFE in steels used in [44] have revealed that the SFE decreases with increasing nitrogen content at low temperatures [45], which is consistent with the inverse proportionality

between SFE and the states density.

5.2. Thermodynamically equilibrium vacancies induced by interstitials. An increase in the equilibrium concentration of vacancies in presence of interstitial atoms was theoretically predicted by McLellan for carbon in the iron austenite [46] and Smirnov for a general case [47]. The first experimental observation of hydrogen-induced superabundant vacancies in hydrides was made by Fukai *et al.* [48], although these authors did not discuss their results in thermodynamical terms. A thermodynamic analysis of hydrogen-induced vacancies in austenitic steels was made in [49], where also the dislocation loops formed in hydrogen-charged austenitic steels after hydrogen degassing have been first time observed.

It is remarkable in this relation that similar defects caused by nitrogen in austenitic steels were observed by Kikuchi *et al.* [50] who has shown that dislocation loops in a CrNi austenitic steel containing 0.5% mass N are formed after ageing at 750°C, *i.e.* after the removal of nitrogen from the solid solution.

Moreover, according to [51], the diffusion of chromium atoms and, correspondingly, precipitation of Cr_2N nitrides is accelerated by nitrogen. Both effects observed by Kikuchi *et al.* were not interpreted by these authors as the effect of vacancies. However, they clearly indicate to the nitrogen-induced superabundant vacancies, which enhance migration of Cr atoms and, becoming non-equilibrium, form vacancy clusters.

Superabundant vacancies were never observed in carbon-containing CrNi austenitic steels, which can be obviously explained by the rather low solubility of carbon in austenite.

5.3. Interaction between dislocations and interstitials. In the austenitic steels, the enthalpy of binding between dislocations and C, N, H atoms is about 0.5 to 0.6 eV [52, 53], 0.7 to 0.9 eV [53, 54] and about 0.1 eV [55, 56], respectively. In ferritic (martensitic) steels, the data correspond to 0.8 eV [57], 0.8 eV [57] and 0.18 eV [58], respectively. These results obtained using mechanical spectroscopy suggest that, in comparison with carbon, the pinning of dislocations by nitrogen atoms in the γ-iron is more effective, whereas there is no difference between pinning of dislocations by carbon and nitrogen in the α-iron. The hydrogen atoms pin dislocations weaker, and the H-pinning of dislocations in the α-iron is a bit stronger than in the γ-iron.

However, these studies did not take into account a possible change in the character of the interstitials-dislocation interaction if interstitial atoms follow dislocations in the course of plastic deformation. As the metallic character of interatomic bonds decreases the shear modulus μ (see [7, 9]), the following consequences are expected for dislocation properties: (i) the decrease in the start stress of the dislocation sources (*e.g.*, $\sigma \approx 2\mu b/L$ for the Frank–Read source); (ii) a decrease in the specif-

ic energy of dislocations, *i.e.* their line tension, $\Gamma \approx (\mu b 2/4\pi)/\log(\Re/5b)$, where $\Re$ is the radius of the dislocation curvature; (iii) a decrease in the distance between the dislocations in the pile-ups, $d \approx \approx (\pi\mu b)/[16(1-\nu)n\sigma]$, where σ is the applied stress.

The second prediction suggests the enhanced mobility of dislocations, while the third one says about a larger number of dislocations n in the pile-ups and, consequently, a higher stress at the leading dislocations, $\tau_l = n\tau$, where τ is an applied stress. Consequently, a microcrack can be opened at lower applied stresses, if the stress at the leading dislocations cannot be relaxed.

These two aspects of dislocation-interstitials interaction should be taken into account depending on the relation between the strain rate and mobility of interstitial atoms. If the interstitial atoms remain essentially immobile during plastic deformation, they pin dislocations and the effectiveness of pinning is controlled by the corresponding binding enthalpy.

The situation is strikingly changed if the interstitial atoms can follow dislocations in the course of plastic deformation. In this case, mobility of dislocations is controlled by a change in the interatomic bonding within the clouds of interstitial atoms around the dislocations. The following measurements using mechanical spectroscopy illustrate this phenomenon (see Figs. 12 and 13).

In absence of relaxation processes, the main contribution to the internal friction background is given by the vibrations of dislocation segments and the value of damping is proportional to the area swept by

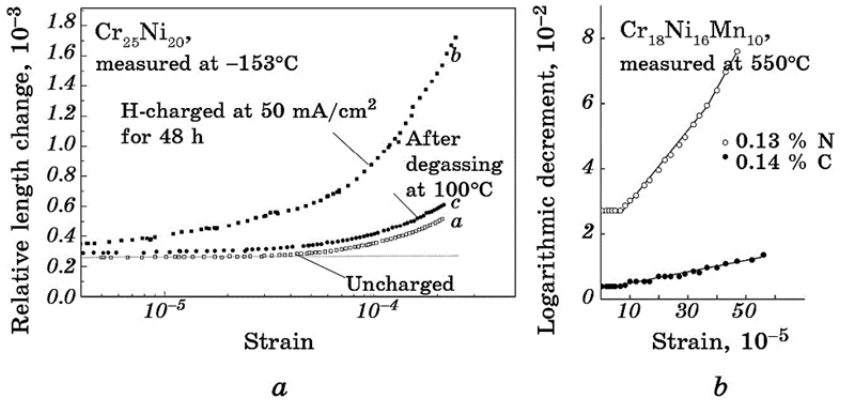

Fig. 12. Effect of interstitial elements on dislocation mobility in austenitic steels measured using strain-dependent internal friction: hydrogen in steel $Cr_{25}Ni_{20}$, *a* is initial state, *b*—after hydrogen charging, *c*—after degassing (*a*); carbon and nitrogen in steel $Cr_{18}Ni_{16}Mn_{10}$; measurements are carried out at elevated temperatures in order to allow the interstitial atoms follow the dislocations (*b*).

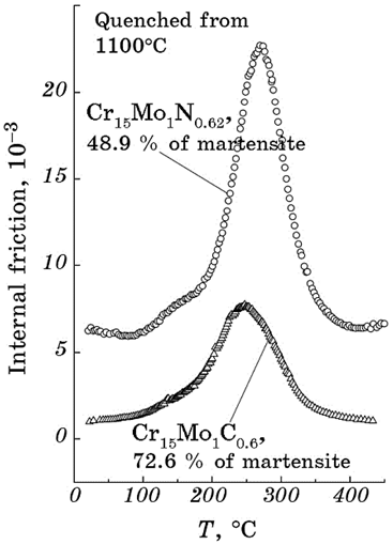

Fig. 13. Effect of carbon and nitrogen on dislocation mobility in martensite of steel $Cr_{15}Mo_1$ measured using the Snoek–Köster relaxation. The fractions of martensite are equal to 72.6% and 48.9% in the carbon and nitrogen steels, respectively.

dislocations for one cycle of vibrations [*e.g.*, 59, 60]. At a constant vibration frequency, it is a measure of dislocation velocity.

The effect of C, N and H on the strain dependence of internal friction is presented in Fig. 12. It is seen that hydrogen charging decreases the stress needed for plastic deformation and increases velocity of dislocations (Fig. 12, *a*). Hydrogen degassing restores the initial IF curve except for a small excess caused by new dislocations induced due to hydrogen charging.

A higher temperature is needed to satisfy conditions of dislocation movement accompanied by the migration of carbon or nitrogen atoms (Fig. 12, *b*). It is clear from the obtained data that, like hydrogen and in contrast to carbon, nitrogen in the austenitic steel increases velocity of dislocations.

The Snoek–Köster (S–K) relaxation provides another possibility to study mobility of dislocations in N, C, or H-containing ferritic or martensitic steels. Exactly like, it is the case for IF background and according to the both compete models of the S–K relaxation [61, 62], the S–K relaxation amplitude is proportional to the area swept by dislocations.

Figure 13 represents the S–K relaxation caused by carbon and nitrogen in the martensite of steels $Cr_{15}Mo_1C_{0.6}$ and $Cr_{15}Mo_1N_{0.62}$. In spite of a significantly smaller fraction of martensite in the nitrogen steel after quenching from 1100°C (48.9% against 72.6% in the carbon

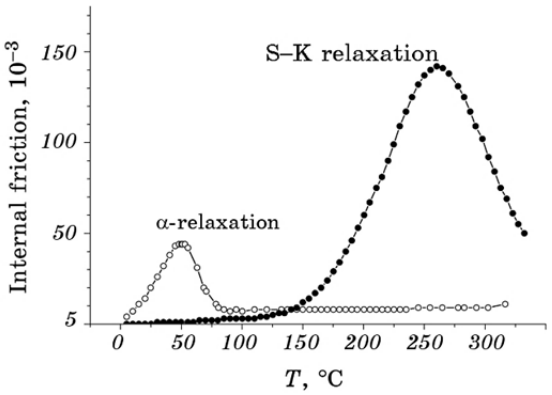

Fig. 14. The α-relaxation in the absence of hydrogen and hydrogen-caused Snoek–Köster relaxation in the α-iron, according to Takita and Sakamoto (according to [63]).

steel), the strength of S–K relaxation caused by the nitrogen-dislocation interaction is much higher.

As follows from the studies by Takita and Sakamoto [63] (see Fig. 14), the strength of hydrogen S–K relaxation in the α-iron is higher by one order of the magnitude than that of the α′-relaxation in the hydrogen-free iron, which is caused by dislocations of the same type as the S–K relaxation in presence of hydrogen.

The presented experimental data clearly show that nitrogen and hydrogen in austenitic and martensitic steels enhance dislocation mobility, whereas carbon decreases it. This unusual behaviour of dislocations moving with the carbon, nitrogen or hydrogen atmospheres can be understood based on the above-mentioned data on the electronic structure of corresponding solid solutions. The nitrogen and hydrogen atoms in the dislocation atmospheres enhance the metallic character of the interatomic bonds, which are weaker than covalent bonds promoted by carbon atmospheres around the dislocations.

6. MECHANICAL PROPERTIES

All of the interstitial elements increase the yield strength of steels except for the hydrogen- and nitrogen-caused softening in the appropriate range of temperatures and strain rates. This unusual phenomenon caused by similar effects of hydrogen and nitrogen on the electronic structure will be discussed in the section devoted to fracture. Presented below is the analysis of carbon and nitrogen effects on the low-temperature and grain-boundary strengthening of austenitic steels.

6.1. Strengthening at low temperatures. An abnormal increase of the

yield strength by nitrogen in the austenitic steels at low temperatures was first time observed by Nilsson and Thorwaldsson [64]. It was ascribed to the nitrogen-caused splitting of the dislocation core in the several slip planes like it occurs in the b.c.c. lattice and a theory of such a b.c.c. behaviour of nitrogen austenitic steels was proposed in [65, 66]. However, more precise measurements were carried out by Nylas and Obst [67] who revealed a three-stage character of the $\sigma(T)$ curve in consistency with Seeger's theory for f.c.c. crystals with low stacking-fault energy smaller than 100 mJ/m^2. According to this theory, because of the absence of strong Peierls barriers for dislocation slip in the f.c.c. crystal lattice, the flow stress is determined by the intersection of dislocations and generation of point defects.

Seeger [68] analysed the following three processes which are responsible for the temperature-dependent flow stress in f.c.c. crystals below the temperature of self-diffusion: (1) interaction between gliding edge dislocations and the forest of dislocations threading the slip plane; (2) interaction between gliding screw dislocations and this forest; (3) thermally activated generation of vacancies by jogs formed during the intersection of screw dislocations. At a given temperature, the plastic flow will be controlled by one of them requiring the lowest stress for the movement of dislocations (Fig. 15, *a*).

In accordance with this theory, the temperatures of the start of thermal activation $T_0^{(1)}$ and $T_0^{(2)}$ for processes (1) and (2) are extremely high. As the process (2) is a prerequisite for the process (3), the one that requires the higher shear stress will control the slip of screw dislocations. Superimposing the curves representing the above three processes results in three sections of the straight lines (see Fig. 15, *b*). Just such a mechanical behaviour of austenitic nitrogen steels was observed by Nyilas *et al.* [67]. Therefore, in accordance with Seeger's theory, depending on the temperature, the operative mechanism for the flow stress is represented by part *1* corresponding to the cutting of edge dislocations through dislocation forest, part *2* from the cutting of screw dislocations through dislocation forest or part *3* controlled by the generation of vacancies by jogs at screw dislocations.

The effect of carbon and nitrogen on the temperature dependence of the yield strength in austenitic steels is presented in Fig. 16. It follows from the comparison with Fig. 15, *b* that the third and first stages of Seeger's scheme, namely the generation of vacancies and the cutting of edge dislocations through the dislocation forest, control the plastic flow at temperatures below 100 K.

The increase of the yield strength in the temperature range of the third stage occurs if nitrogen or carbon is added to the austenitic CrNiMn steel, and the effect of nitrogen is much higher. Thus, the intersection of screw dislocations and, namely, the generation of vacancies by the jogs discern the low-temperature mechanical behaviour of

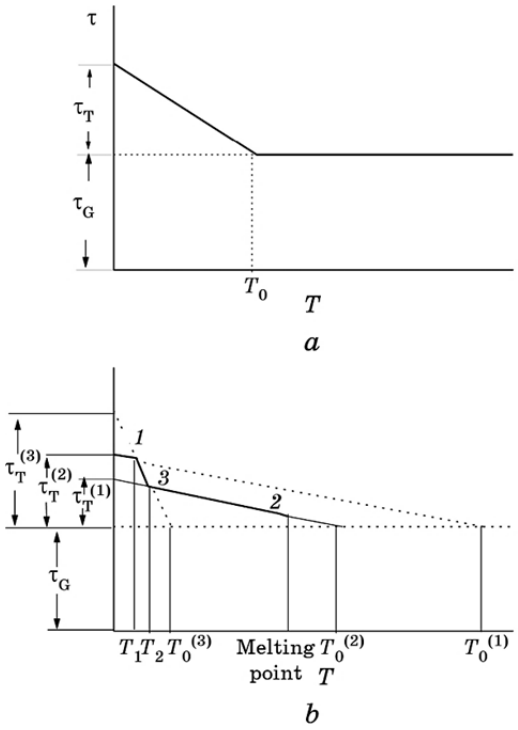

Fig. 15. Flow stress versus temperature for f.c.c. crystals with a low value of stacking fault energy, according to Seeger's theory [68]: if only one thermally activated process is operating (*a*); for three controlling mechanisms of plastic deformation: cutting of edge (*1*) and screw (*2*) dislocations through the dislocation forest and generation of vacancies by jogs in screw dislocations (*3*), as predicted to occur in the crystals with low stacking-fault energy (*b*).

three studied steels. The generation of vacancies by jogs requires, as a preceding stage, the formation of a constriction in the extended dislocations. The more split dislocations, the higher stress has to be applied to form the constriction. Therefore, the nature of the different mechanical behaviour of the studied steels in stage *3* controlled by different splitting of dislocations at low temperatures. In other words, carbon and nitrogen change the temperature dependence of the stacking fault energy to a different degree.

This suggestion was confirmed by the low-temperature TEM studies [69]. It was obtained that, in contrast to carbon, nitrogen strikingly decreases the SFE at low temperatures, which results in a larger applied stress for the formation of constriction in the intersecting screw dislocations.

A reason for the nitrogen-caused change in the temperature dependence of the SFE lies in the increased states density at the Fermi level

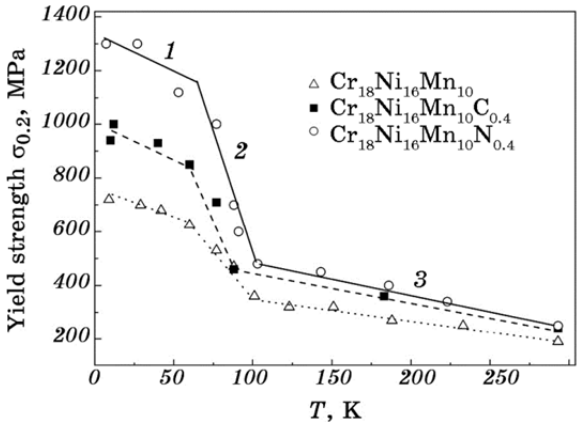

Fig. 16. Effect of nitrogen and carbon on the temperature dependence of the yield strength of austenitic steel $Cr_{18}Ni_{16}Mn_{10}$. Stages *1* to *3* controlling different mechanisms of plastic flow are shown in consistency with Seeger's theory [68].

(see Fig. 1). With decreasing temperature, the temperature-caused blurring of the Fermi level is decreased and, consequently, the states' density increases, which is accompanied by decreasing SFE in accordance with the inverse proportionality between the states density at the Fermi level and the SFE [37]. The low-temperature increase of the yield strength in the carbon austenitic steels is rather small because of the weak temperature dependence of the SFE resulted from prevailing covalent bonds and the low states' density at the Fermi level.

One can suppose that, like nitrogen, hydrogen is expected to strikingly increase the yield strength at low temperatures because of strong increase in the states density at the Fermi level in hydrogen-charged austenitic steels.

6.2. Strengthening by grain boundaries. Nitrogen is found to increase more effectively the grain-boundary strengthening in austenitic steels as compared to carbon (see Fig. 17). Three main theories, namely those of planar slip [72], cold work [73] and grain-boundary dislocation sources [74], were proposed for the interpretation of the Hall–Petch equation $\sigma_T = \sigma_0 + kd^{-1/2}$ where σ_T is the yield strength, σ_0 is the friction stress of the lattice, d is the grain size and k is a coefficient characterising the transfer of the slip through the grain boundary. As follows from Fig. 17, nitrogen increases the coefficient k.

Nitrogen austenitic steels are a unique object for testing the abovementioned theories of grain-boundary strengthening (see about details [53]). Main experimental data are the following.

Unlike carbon, nitrogen assists the planarity of slip in austenitic steels, which was first time shown in [75]. Therefore, if planar slip

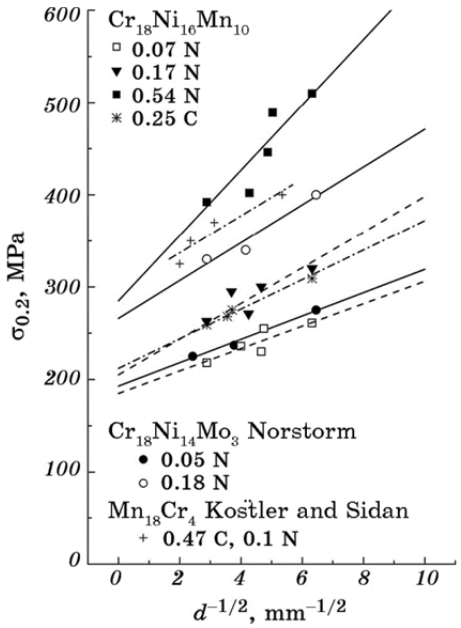

Fig. 17. Effect of nitrogen and carbon on grain boundary strengthening of steel $Cr_{18}Ni_{16}Mn_{10}$. Data of Norström [70] for steel $Cr_{18}Ni_{14}Mo_3$ alloyed with nitrogen and of Köstler and Sidan [71] for steel $Mn_{18}Cr_4$ alloyed with carbon are shown for the comparison.

controls the value of k, it has to be decreased with increasing nitrogen content because a critical stress at the head of the pile-ups needed for the slip transfer to adjacent grains could be achieved at smaller applied stresses. Such an idea is in contradiction with numerous experimental data.

The cold work theory [73] explains the Hall–Petch equation in terms of increased dislocation density at the grain boundaries with decreasing the grain size, which makes more difficult the slip transfer through the grain boundary (see also experimental data in [76]). Nitrogen increases the cold-work hardening in austenitic steels [77, 78], which is consistent with the increase of k expected according to the cold work theory.

Nevertheless, no contribution of nitrogen to the cold-work hardening occurs in steel with basic composition of $Cr_{18}Ni_{16}Mn_{10}$ [53], and, at the same time, as shown in Fig. 17, the coefficient k in this steel increases with increasing nitrogen content. Therefore, the increase in the density of dislocations near the grain boundary with decreasing grain size is not critical for the grain-boundary strengthening, at least for the yield strength.

The theory of the grain-boundary dislocation sources attributes the

Hall–Petch relationship to the long-range internal stresses caused by the dislocations located within the grain boundaries. The only experimental evidence supporting this theory is that the grain-boundary segregation of solute atoms contributes to the grain-boundary strengthening. However, the experimental data about a weak segregation of nitrogen [79] and remarkable segregation of carbon [80] at the grain boundaries in austenitic steels are not consistent with the supposed decisive role of the grain-boundary dislocation sources.

Possibly, the idea proposed by Cottrell [81] as far back as in the fifties that the coefficient k is controlled by the stress needed for unpinning the dislocation sources in the adjacent grain still remains the most fruitful for the interpretation of the Hall–Petch equation. A larger binding enthalpy of dislocations to nitrogen than to carbon in austenitic steels is consistent with this Cottrell's idea except for the only remark that the slip planarity is not necessary condition for the grain-boundary strengthening.

Hydrogen is notoriously known by its strong affinity with the grain boundaries. In view of hydrogen-caused embrittlement, its role in grain-boundary strengthening is not worth of detailed studies.

6.3. Fracture. Carbon decreases the toughness of austenitic steels; however, it does not cause the ductile-to-brittle transition. The excellent combination of strength and toughness in nitrogen austenitic steels was firstly shown in [82]. At the same time, the ductile-to-brittle transition occurs in the impact tests at the nitrogen contents higher than $\cong 0.8\%$ mass [83, 84]. Numerous observations of the fracture surface reveal a surprising similarity between the low-temperature impact embrittlement of nitrogen austenitic steels and hydrogen brittleness (see Fig. 18 and [85–87]). In contrast, no ductile-to-brittle transition occurs in carbon austenitic steels.

As shown by Tomota *et al.* [87], the brittleness of nitrogen austenitic steels under low-temperature impact loading is resulted from the nitrogen-enhanced highly localized plasticity and shortage of time for the relaxation of stresses. Similarly, the hydrogen-enhanced localized plasticity is one of the most reliable hypotheses of hydrogen embrittlement (*e.g.*, [3]). Based on the similar effect of nitrogen and hydrogen on the electronic structure of austenitic steels, one can state that the N- and H-caused macrobrittleness is of the same physical nature and originates from the increase in the concentration of free electrons and the excessive electron density within the nitrogen and hydrogen atmospheres around the dislocations [56].

Unlike hydrogen, nitrogen atoms in austenite are immobile at room temperature, and this is why the common tension tests do not reveal the nitrogen-caused embrittlement. However, at high strain rates, the interstitial atoms are transported by dislocations even at cryogenic temperatures like those that it was shown in [88] using autoradiog-

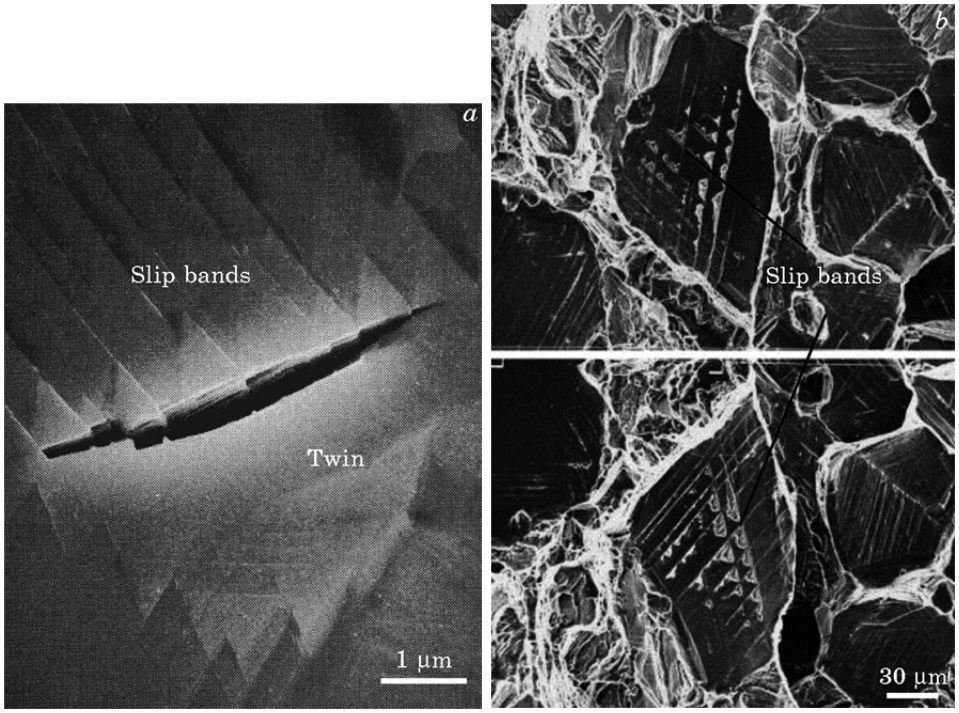

Fig. 18. Hydrogen- and nitrogen-caused fracture of austenitic steels: hydrogen-caused slip bands resulted in cracking at a twin boundary (after [85]) (*a*), mirror surfaces of steel $Cr_{18}Mn_{18}N_{0.6}$ after pseudo-brittle fracture during the low-temperature impact test (after [87]) (*b*).

raphy.

The nature of slip localization due to nitrogen and hydrogen is of different type. The slip in the nitrogen austenite is localized due to short-range atomic order [19]. Hydrogen cannot change the distribution of substitutional solutes, at least at the room temperature hydrogenation. Therefore, some other reason has to exist for the hydrogen-caused localisation of slip within the separate bands. A mechanism related with the hydrogen-induced vacancies has been proposed to be responsible for the hydrogen-caused slip localisation [6, 56]. It is similar to the voids sheeting analysed by Ashby *et al.* [89]. Like the microvoids, the hydrogen-induced vacancies within the hydrogen atmospheres around dislocations decrease the load-bearing area in the slip plane, which results in slip localization.

7. CONCLUSIONS

1. Change in the atomic interactions determines the structure and

properties of the iron-based solid solutions containing carbon, nitrogen or hydrogen. Carbon decreases the concentration of free electrons, whereas nitrogen and hydrogen increase it.
2. Carbon increases and hydrogen decreases the stacking fault energy of austenitic steels. With increasing nitrogen content, stacking fault energy is being changed non-monotonously.
3. Carbon promotes clustering of solute atoms in austenitic solid solutions, whereas nitrogen assists the short-range atomic ordering.
4. All these elements increase the thermodynamically equilibrium concentration of vacancies in the γ-iron solid solution and assist migration of substitutional solutes.
5. Dislocations in austenitic steels are more effectively pinned by nitrogen than carbon. Pinning of dislocations by hydrogen is insignificant. At the same time, if the clouds of interstitial atoms can follow dislocations in the course of deformation, the nitrogen and hydrogen atoms enhance plasticity due to excessive free electron concentration in the dislocation atmospheres, *i.e.* prevailing metallic character of interatomic bonds and, consequently, decreased line tension of dislocations.
6. Abnormal strengthening of nitrogen austenitic steels at low temperatures is explained based on the nitrogen-increased concentration of free electrons resulting in the striking temperature dependence of stacking fault energy. A similar effect is expected for hydrogen-charged austenitic steels and not for carbon ones.
7. The pseudo-brittle fracture of nitrogen- and hydrogen-containing austenitic steels occurs at the conditions of dislocation slip accompanied by the migration of nitrogen or hydrogen atoms. This phenomenon is attributed to the local H- and N-increased concentration of free electrons and superabundant vacancies leading to the enhanced microplasticity and localization of plastic deformation.

REFERENCES

1. V. G. Gavriljuk and H. Berns, *High Nitrogen Steels* (Berlin: Springer Verlag: 1999).
2. H. Berns, V. G. Gavriljuk, and S. Riedner, *High Interstitial Stainless Steels* (Heidelberg: Springer: 2013).
3. H. K. Birnbaum and P. Sofronis, *Mat. Sci. Eng. A*, **176**: 191 (1994).
4. S. P. Lynch, *Acta Metall.*, **36**, No. 10: 2639 (1988).
5. M. Nagumo, *ISIJ Intern.*, **41**, No. 6: 590 (2011).
6. V. G. Gavriljuk, B. D. Shanina, V. N. Shyvanyuk, and S. M. Teus, *Corrosion Rev.*, **31**, No. 2: 33 (2013).
7. S. M. Teus, V. N. Shyvanyuk, B. D. Shanina, and V. G. Gavriljuk, *phys. status solidi (a)*, **204**, No. 12: 4249 (2007).
8. D. N. Movchan, V. N. Shyvanyuk, B. D. Shanina, and V. G. Gavriljuk, *phys. status solidi (a)*, **207**, No. 8: 1796 (2010).

9. V. G. Gavriljuk, B. D. Shanina, V. N. Syvanyuk, and S. M. Teus. *J. Appl. Phys.*, **108**: 083723 (2010).
10. V. G. Gavriljuk, B. D. Shanina, N. P. Baran, and V. M. Maximenko, *Phys. Rev. B*, **48**, No. 5: 3224 (1993).
11. B. D. Shanina, S. P. Kolesnik, A. A. Konchitz, V. G. Gavriljuk, S. Yu. Smouk, and A. V. Tarasenko, *Solid State Commun.*, **90**, No. 2: 109 (1994).
12. B. D. Shanina, V. G. Gavriljuk, A. A. Konchitz, S. P. Kolesnik, and A. V. Tarasenko, *phys. status solidi (a)*, **149**, No. 2: 711 (1995).
13. B. D. Shanina, V. G. Gavriljuk, S. P. Kolesnik, and V. N. Shivanyuk, *J. Phys. D: Appl. Phys.*, **32**: 298 (1999).
14. W. Seith, *Diffusion in Metallen, Platzwechselreaktionen* (Berlin–Göttingen–Heidelberg: Springer-Verlag: 1955).
15. H. Nakajima and K. Hirano, *ISIJ Intern.*, **19**: 400 (1978).
16. A. L. Sozinov, A. G. Balanyuk, and V. G. Gavriljuk, *Acta Mater.*, **45**, No. 1: 225 (1997).
17. A. L. Sozinov, A. G. Balanyuk, and V. G. Gavriljuk, *Acta Mater.*, **47**, No. 3: 927 (1999).
18. A. G. Balanyuk, V. G. Gavriljuk, V. N. Shivanyuk, A. I. Tyshchenko, and J. Rawers, *Acta Mater.*, **48**, No. 15: 3813 (2000).
19. V. G. Gavriljuk, B. D. Shanina, and H. Berns, *Acta Mater.*, **48**, No. 15: 3879 (2000).
20. B. Shanina, V. Gavriljuk, H. Berns, and F. Schmalt, *Steel Research*, **73**, No. 3: 105 (2002).
21. V. G. Gavriljuk, B. D. Shanina, and H. Berns, *Acta Mater.*, **56**: 5071 (2008).
22. J. H. Pifera and R. T. Longo, *Phys. Rev. B*, **4**: 3797 (1971).
23. V. G. Gavriljuk, A. L. Sozinov, A. G. Balanyuk, S. V. Grigoriev, O. A. Gubin, G. P. Kopitsa, A. I. Okorokov, and V. V. Runov, *Mater. Trans. A*, **28**, No. 11: 2195 (1997).
24. I. I. Gurevich and T. V. Tarasov, *Physics of Low Energy Neutrons* (Moscow: Nauka: 1965) (in Russian).
25. B. D. Shanina, V. G. Gavriljuk, A. A. Konchitz, and S. P. Kolesnik, *J. Phys.: Condens. Matter*, **10**: 1825 (1998).
26. H. Thier, A. Bäumel, und E. Schmidtmann, *Arch. Eisenhüttenwesen*, **40**, No. 4: 333 (1969).
27. U. Heubner, M. Rockel, und E. Wallis, *Werkstoffe und Korrosion*, **40**: 459 (1989).
28. S. Hertzman, *Scand. J. Metallurgy*, **24**: 140 (1995).
29. R. F. A. Jargelius-Pettersson, *Z. Metallkd.*, **89**, No. 3: 177 (1998).
30. H. Berns, V. A. Duz', R. Ehrhardt, V. G. Gavriljuk, and A. V. Tarasenko. *Metallofiz. Noveishie Tekhnol.*, **15**: 561 (1995) (in Russian).
31. H. Berns, V. A. Duz', R. Ehrhardt, V. G. Gavriljuk, Yu. N. Petrov, and A. V. Tarasenko, *Z. Metallkd.*, **88**, No. 2: 109 (1997).
32. A. Szumer and A. Janko, *Corrosion*, **35**: 461 (1979).
33. A. Inoue, Y. Hosoya, and T. Masumoto, *ISIJ Intern.*, **19**: 170 (1979).
34. N. Narita, C. J. Altstetter, and H. K. Birnbaum, *Metall. Trans. A*, **13**: 1355 (1982).
35. A. G. Vakhney, A. N. Yaresko, V. N. Antonov, V. V. Nemoshkalenko, V. G. Gavriljuk, V. A. Tarasenko, and I. Smurov, *J. Phys.: Condens. Matter*, **10**: 6987 (1998).

36. D. N. Movchan, B. D. Shanina, and V. G. Gavriljuk, *Int. J. Hydrogen Energy*, **38**: 8471 (2013).
37. N. I. Noskova, V. A. Pavlov, and S. A. Nemnonov, *Fiz. Met. Metalloved.*, **20**, No. 6: 920 (1965) (in Russian).
38. R. E. Schramm and R. P. Reed, *Metall. Trans. A*, **6**: 1345 (1975).
39. A. E. Pontini and J. D. Hermida, *Scr. Mater.*, **37**: 1831 (1997).
40. R. Fawley, M. A. Quader, and R. A. Dodd, *Trans. TMS AIME*, **242**: 771 (1968).
41. P. R. Swann, *Corrosion*, **19**, No. 3: 102 (1963).
42. D. Dulieu and J. Nutting, *Metallurgical Developments in High-Alloy Steels Proc.* (London: Iron and Steel Institute: 1964), p. 140.
43. R. E. Stoltz and J. B. Vander Sande, *Metall. Trans. A*, **11**, No. 6: 1033 (1980).
44. V. Gavriljuk, Yu. Petrov, and B. Shanina, *Scr. Mater.*, **55**: 537 (2006).
45. V. G. Gavriljuk, A. L. Sozinov, J. Foct, Yu. N. Petrov, and A. A. Polushkin, *Acta Mater.*, **46**, No. 4: 1157 (1998).
46. R. B. McLellan, *J. Phys. Chem. Sol.*, **49**: 1213 (1988).
47. A. M. Bobyr, V. N. Bugaev, and A. A. Smirnov, *Doklady Akad. Nauk USSR*, **320**: 1113 (1991) (in Russian).
48. Y. Fukai and N. Okuma, *Jpn. J. Appl. Phys.*, **32**, No. 2: L1256 (1993).
49. V. G. Gavriljuk, V. N. Bugaev, Yu. N. Petrov, A. V. Tarasenko, and B. Z. Yanchitsky, *Scr. Mater.*, **34**, No. 6: 903 (1996).
50. M. Kikuchi, T. Tanaka, and R. Tanaka, *Metall. Trans.*, **5**, No. 6: 1520 (1974).
51. M. Kikuchi, *Proc. University of Tokyo–Harbin Institute of Technology Symposium on Materials Science (May 20–22, 1985)* (Tokyo: 1985), p. 22.
52. V. G. Gavriljuk, V. A. Duz', S. P. Yefimenko, and O. G. Kvasnevsky, *Fiz. Met. Metalloved.*, **64**, No. 6: 1132 (1987) (in Russian).
53. V. G. Gavriljuk, V. A. Duz', and S. P. Yephimenko, *Proc. of 1st Intern. Conf. 'High Nitrogen Steels' (May 18–20, 1988)* (London: Institute of Metals: 1989), p. 447.
54. V. G. Gavriljuk, H. Berns, Ch. Escher, N. I. Glavatska, A. Sozinov, and Yu. N. Petrov, *Mat. Sci. Eng. A*, **271**: 14 (1999).
55. A. Atrens, N. F. Fiore, and K. Miura, *J. Appl. Phys.*, **48**: 4247 (1977).
56. V. G. Gavriljuk, B. D. Shanina, V. N. Shyvanyuk, and S. M. Teus, *Proc. of the 2012 International Hydrogen Conference (September 9–12, 2012, Wyoming)* (New York: ASME Press: 2014), p. 67.
57. V. G. Gavriljuk, N. P. Kushnareva, and V. G. Prokopenko, *Fiz. Met. Metalloved.*, **42**, No. 6: 1288 (1976) (in Russian).
58. A. Zelinski, E. Lunarska, and M. Smialowski, *Acta Metall.*, **25**: 551 (1977).
59. G. Schoeck, E. Bisogni, and J. Shyne, *Acta Metall.*, **12**: 1466 (1964).
60. A. Rivière, J. P. Amirault, and J. Woirgard, *Il Nuovo Cimento*, **33**: 398 (1976).
61. G. Schoeck, *Acta Metall.*, **11**: 617 (1963).
62. A. Seeger, *phys. status solidi (a)*, **55**: 457 (1979).
63. K. Takita and K. Sakamoto, *Scr. Metall.*, **10**, No. 5: 399 (1976).
64. J.-O. Nilsson and T. Thorwaldsson, *Scand. J. Metallurgy*, **15**: 83 (1985).
65. M. Grujicic, *Mater. Sci. Eng. A*, **183**: 223 (1994).
66. M. Grujicic and X. W. Zhou, *Mater. Sci. Eng. A*, **190**: 8 (1995).
67. A. Nyilas, B. Obst, and H. Nakajima, *Proc. 3rd Intern. Conf. 'High Nitrogen Steels' (September 14–16, 1993)* (Eds. V. G. Gavriljuk and V. M. Nadutov) (Kiev: Institute for Metal Physics: 1993), p. 339.
68. A. Seeger, *Philos. Mag.*, **46**, No. 382: 1194 (1955).

69. V. G. Gavriljuk, A. L. Sozinov, J. Foct, Yu. N. Petrov, and A. A. Polushkin, *Acta Mater.*, **46**, No. 4: 1157 (1998).
70. L. A. Norström, *Metal Sci.*, **11**, No. 6: 208 (1977).
71. H. J. Köstler und H. Sidan, *Z. Wirtsch Fert*, **72**, No. 10: 785 (1977).
72. N. J. Petch, *J. Iron Steel Inst.*, **174**: 25 (1953).
73. H. Conrad, *Acta Metall.*, **11**, No. 1: 75 (1963).
74. J. C. M. Li, *Trans TMS AIME*, **227**, No. 2: 239 (1963).
75. J. Sassen, A. J. Garrat-Reed, and W. S. Owen, *Proc. of 1st Intern. Conf. 'High Nitrogen Steels' (May 18–20, 1988)* (London: Institute of Metals: 1989), p. 159.
76. B. P. Kashyap and K. Tangri, *Acta Metall. Mater.*, **43**, No. 11: 3971 (1995).
77. N. D. Afanasyev, V. G. Gavriljuk, V. A. Duz', V. L. Svechnikov, and V. M. Nadutov, *Fiz. Met. Metalloved.*, **8**: 121 (1990) (in Russian).
78. P. J. Uggowitzer and M. O. Speidel, *Proc. 2nd Intern. Conf. 'High Nitrogen Steels' (October 10–12, 1990)* (Düsseldorf: Stahl und Eisen: 1990), p. 156.
79. Yu. N. Petrov, V. G. Gavriljuk, H. Berns, and Ch. Escher, *Scr. Mater.*, **40**, No. 6: 69 (1999).
80. Yu. N. Petrov, *Scr. Metall. Mater.*, **29**: 1471 (1993).
81. A. H. Cottrell, *Trans. TMS–AIME*, **212**: 192 (1958).
82. J. Frehser und Ch. Kubisch, *Berg und Hüttenmännische Monatshefte*, **108**, No. 11: 369 (1963).
83. M. A. E. Harzenmoser, *Massive Aufgestickte Austenitisch-Rostfreie Stähle und Duplexstähle* (Thesis of Disser. for Dr. Sci.) (Zürich: Eidgenössische Technische Hochschule: 1990).
84. P. J. Uggowitzer, N. Paulus, and M. O. Speidel, *Application of Stainless Steels'92* (Stockholm: The Institute of Metals: 1992), p. 62.
85. D. G. Ulmer and C. J. Altstetter, *Acta Metall. Mater.*, **39**: 1237 (1991).
86. H. Hänninen and T. Hakkarainen, *Metal. Trans. A*, **10**: 1196 (1979).
87. Y. Tomota, Y. Xia, and K. Inoue, *Acta Mater.*, **46**, No. 5: 1577 (1998).
88. V. G. Gavriljuk, D. S. Hertsricken, V. M. Falchenko, and Yu. A. Polushkin, *Fiz. Met. Metalloved.*, **51**, No. 1: 147 (1981) (in Russian).
89. D. Teirlinck, F. Zok, J. D. Embury, and M. F. Ashby, *Acta Metall.*, **36**, No. 5: 1213 (1988).